Resonant two-photon ionization spectroscopy of jet-cooled NiPt

Scott Taylor, Eileen M. Spain, and Michael D. Morse
Department of Chemistry, University of Utah, Salt Lake City, Utah 84112

(Received 6 September 1989; accepted 10 November 1989)

Resonant two-photon ionization spectroscopy of jet-cooled NiPt has been used to investigate the possibility of *d*-electron contributions to the bonding in this species. Based on an abrupt onset of predissociation, the bond strength of NiPt is assigned as $D_0(\mathrm{NiPt}) = 2.798 \pm 0.003$ eV. Comparisons of scans using ArF (6.42 eV) or F_2 (7.87 eV) radiation as the ionization laser yield IP(NiPt) $= 8.02 \pm 0.15$ eV, from which we derive $D_0(\mathrm{Ni^+–Pt}) = 2.41 \pm 0.15$ eV and $D_0(\mathrm{Ni–Pt^+}) = 3.58 \pm 0.35$ eV. High resolution studies of the 6–0 and 8–0 bands of one of the three identifiable progressions demonstrate an $\Omega' = 0 \leftarrow \Omega'' = 0$ transition with $r_e' = 2.3396 \pm 0.0039$Å and $r_0'' = 2.2078 \pm 0.0023$Å. The short bond length and large bond strength of NiPt, as compared to the corresponding values ($r_e = 2.330 \pm 0.003$Å and $D_0 = 2.34 \pm 0.10$ eV) for the coinage metal analog, CuAu, demonstrate significant *d*-orbital contributions to the bonding in NiPt.

I. INTRODUCTION

One of the most important questions concerning the electronic structure and chemistry of the transition metals is the role that the *d*-orbitals play in the metal–metal and metal–ligand chemical bonding. The presence of energetically accessible *d*-orbitals is, after all, what distinguishes the transition metals from the rest of the periodic table, leading to the remarkable physical and chemical properties which are associated with this group of metals. The accessible *d*-orbitals of the transition metals are ultimately responsible for such varied phenomena as the incredible strength and high melting points of tungsten, tantalum, and molybdenum (as compared to the main group metals); the ferromagnetic behavior of iron, cobalt, and nickel; the diversity of stable oxidation states of the transition metals; and the variety of processes which may be catalyzed by transition metals and their compounds.

The contribution of the *d*-orbitals to the metal–metal bond has been an active field of research ever since multiply-bonded ligated metal dimers were discovered in the mid-1960's.[1] More recently, however, both experimental[2,3] and theoretical[4–7] methods have been used to investigate the chemical bonding in transition metal dimers and higher clusters, without the benefit of stabilizing ligands. This interest is warranted due to the important role the transition metals play in metallurgy and materials science, solid state physics, and heterogeneous catalysis. In principle, the simplest systems displaying metal–metal bonds which might have *d*-orbital contributions are the transition metal dimers, which may be considered prototypes for understanding the metal–metal chemical bond. Through the accumulation of experimental data on these systems we hope to establish the foundation of knowledge from which generalizations may be drawn, ultimately providing a unified picture of metal–metal bonding among the transition metals.

Such a grand scheme is not all that motivates experiments on the transition metal dimers. Theoretical chemists continue to develop and refine quantum mechanical methods, and with the growing availability of supercomputers have chosen to attack problems of ever-increasing complexity. The open *d*-shell transition metal dimers are certainly in this category, and continue to present a formidable challenge to *ab initio* theory. In these systems exchange and correlation effects can be considerable, and spin–orbit interactions and other relativistic effects may be quite significant as well. The sheer number of low-lying excited states serves to make the configuration interaction method difficult at best, and often nearly intractable. With such major difficulties in the theoretical treatment of metallic systems, experiment fulfills the crucial role of determining fundamental physical quantities such as bond lengths, dissociation energies, and term symbols, thereby providing a reference point for testing the validity of various calculational methods. On the other hand, it is the theoretician who must ultimately provide the detailed description of metal electronic structure. Most importantly, it is the theoretical chemist who will provide the language and conceptual framework for understanding the electronic structure of metals.

In previous studies of diatomic transition metals, *d*-orbital contributions to the bonding of V_2[8], Cr_2[9–12], and Mo_2[13–15] have been clearly demonstrated by the extremely short bond lengths of these molecules in their ground electronic states: 1.77, 1.679, and 1.938 Å, respectively. Likewise, *d*-electron bonds in Ti_2 may be inferred from the high vibrational frequency of 407.9 $\mathrm{cm^{-1}}$, as measured by resonance Raman spectroscopy of Ti_2 isolated in argon matrices.[16] The sizeable bond strength of Nb_2, given by various investigators as 5.19 ± 0.28[17], 5.57 ± 0.41[18], or 5.22 ± 0.02 eV[18] also provides evidence of strong *d*-electron participation in the chemical bonding in diatomic niobium. On the other hand, the contribution of *d* electrons to the chemical bonding in Cu_2, Ag_2, and Au_2 is essentially nil, since these elements have ground atomic states of $nd^{10}(n+1)s^1, {}^2S$. In such cases promotion of an *nd* electron to the $(n+1)p$ shell could in principle enable a triple bond to be formed,[19] but there is no evidence that such configurations are important in the ground states of the coinage metal dimers.[20] The promotion energy required for opening the closed *d*-shell is simply too high for such effects to be important.

An important determinant of the electronic structure of

 0021-9606/90/052698-12$03.00

the transition metal dimers is the relative orbital sizes of the *nd* and $(n+1)s$ atomic orbitals.[21] It is well known that as one moves across the transition metal series the increased nuclear charge causes the *nd* orbitals to contract significantly. On the other hand, the additional *nd* electrons are quite effective in shielding the outer $(n+1)s$ electrons from the added nuclear charge, resulting in a much less dramatic contraction of the $(n+1)s$ orbital as compared to the *nd* orbitals. As a result of this differential contraction, the overlap between *nd* orbitals on two adjacent metal centers becomes less significant as one moves to the right in the transition metal series. Thus, among the open *d*-shell transition metal dimers, Ni_2, Pd_2, and Pt_2 would be expected to have the smallest contribution from *d–d* bonding of the homonuclear diatomics of their respective rows. This expectation has proven to be correct for Ni_2[22], which exhibits a bond length and dissociation energy (2.200 ± 0.007Å and 2.068 ± 0.01 eV, respectively)[22] within 3% of the accepted values for Cu_2 (2.2197Å[23] and 2.01 ± 0.08 eV[3], respectively). On the other hand, Pt_2 shows a very significant degree of *d*-orbital contributions to the bonding, as evidenced by a comparison of its bond strength (3.14 ± 0.02 eV)[24] to that of Au_2 (2.29 ± 0.02 eV).[25]

Given the importance of 5*d* contributions to the bonding in Pt_2, it is now evident that the 5*d* orbitals are important in the chemical bonding of all the open 5*d*-shell transition metals. In this respect the third transition metal series differs dramatically from the first, primarily because the 5*d* and 6*s* orbitals are more nearly equal in size than are the 3*d* and 4*s* orbitals. As a result, the 5*d* orbitals are quite accessible for chemical bonding, even at the right side of the periodic table where they are most tightly contracted.

With this distinction between the 3*d* and 5*d* metals in mind, a question naturally arises: In diatomic NiPt, will the chemical bonding be similar to Ni_2, with little if any contribution from *d*-electron bonding, or will the large 5*d* orbitals of platinum somehow find the 3*d* (or 4*p*) orbitals of nickel, resulting in a bond strength significantly greater than that of the filled *d*-shell and analog, CuAu? What is the electronic structure of NiPt, and how does it compare to Ni_2 ant Pt_2? To answer these questions an investigation of NiPt was undertaken, the results of which are presented here.

The experimental aspects of this study are presented in Sec. II, while Sec. III contains the results. The experimental findings are discussed in Sec. IV, where further comparisons between NiPt, Ni_2, and Pt_2, and coinage metal dimers are made. Section V concludes the paper with a summary of our most significant results.

II. EXPERIMENTAL

The supersonic cluster beam apparatus employed in the present study is essentially the same as that used in previous investigations of Pt_2,[24] NiCu,[26] C_3,[27] and Al_3[28] in this laboratory. A pulsed supersonic beam of platinum group metal clusters is produced by laser vaporization of a custom-made alloy disk composed of equimolar proportions of Ni, Pd, and Pt (Alfa, $1.0 \times 25 \times 25$ mm, 99.9% purity) located in the throat of a pulsed supersonic nozzle. In the present investigation vaporization is achieved by focusing the second harmonic radiation (532 nm, 30–50 mJ/pulse) of a *Q*-switched Nd:YAG laser onto the alloy disk, which is continuously rotated and translated using a rotating disk assembly similar to that described by O'Brien *et al.*[29] The vaporization laser is timed to coincide with the peak density of helium carrier gas, which is pulsed over the target by a magnetically operated double solenoid valve.[15] The high pressure of helium (8 atm in the reservoir behind the pulsed valve) flows through a 2 mm diameter channel over the target, quenching the hot metal plasma, thereby allowing clusters to form. Formation of NiPd, NiPt, and PdPt is facilitated by attaching a small extender to the nozzle, which provides a volume (approximately 0.5 cm^3) in which further clustering occurs. This is followed by a 1 mm orifice, from which the clusters expand into vacuum. The resulting supersonic expansion is then skimmed, after which it enters the ionization region of a reflectron-type time-of-flight mass spectrometer.

Ionization of the metal cluster beam was achieved by non-resonant two-photon ionization using high-intensity ArF (193 nm, 20 mJ/cm^2) radiation to optimize the cluster signal. Subsequent spectroscopic experiments were conducted using the resonant two-photon ionization (R2PI) technique, in which one photon was absorbed from a scanning dye laser and ionization was achieved by absorption of a second photon from an excimer laser operating on ArF. High resolution studies were carried out using an intracavity etalon and accessories (Molectron, DL 224), which was pressure scanned from 0 to 1 atm using SF_6. Absolute frequency measurements were made by simultaneously monitoring the absorption spectrum of gaseous I_2, which was then compared to the iodine atlas.[30,31] In the course of this investigation the dye laser was operated using all of the following dyes: stilbene 420; coumarins 440, 460, 480, 500, and 540A; rhodamines 590, 610, and 640; DCM; and LDS dyes 698, 750, 751, 765, 821, 867, and 925 (all obtained from Exciton).

III. RESULTS

A. Mass spectra

Mass spectra obtained by ArF (193 nm, 6.42 eV) and F_2 (157 nm, 7.9 eV) photoionization of the metal clusters formed by laser vaporization of the equimolar mix of nickel, palladium, and platinum showed a high intensity of the atomic species, along with all six diatomics, Ni_2, NiPd, Pd_2, NiPt, PdPt, and Pt_2. Triatomic species, including Ni_3, $NiPd_2$, Ni_2Pt, and NiPdPt were also present in the mass spectrum. Conditions were optimized for production of NiPt, resulting in a well-resolved mass spectrum which is depicted in Fig. 1. The relative peak heights of the individual masses are consistent with the natural abundances of Ni and Pt, as shown in Table I.

As is indicated in Table I, of the intense features in the mass spectrum, masses 252 and 253 are nearly isotopically pure. These masses are 99.09% $^{58}Ni^{194}Pt$ and 99.96% $^{58}Ni^{195}Pt$, respectively. The reduced masses for these species differ by only 0.12%, so very little isotope shift is expected. On the other hand, the mass 254 feature is composed of 66.48% $^{58}Ni^{196}Pt$ and 33.41% $^{60}Ni^{194}Pt$. These species dif-

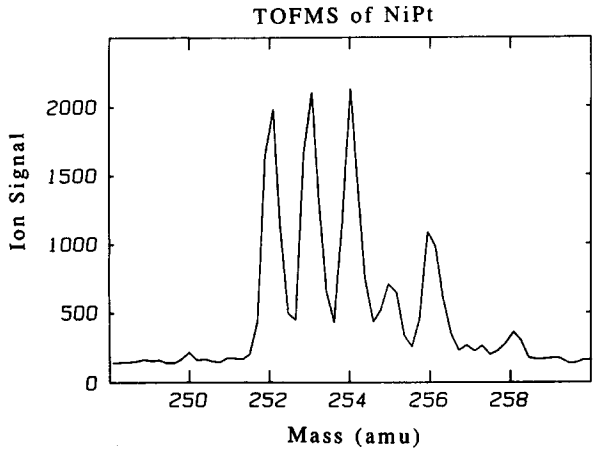

FIG. 1. Resonant two-photon ionization mass spectrum of the NiPt molecule, showing all isotopes clearly resolved. The intensity pattern of the observed isotopes is exactly as expected for this species (compare Table I), and identifies it unambiguously as diatomic NiPt. This mass spectrum was obtained by blocking the oscillator cavity of a dye laser operating on rhodamine 610, and allowing amplified spontaneous emission to excite all isotopic combinations of NiPt. Ionization was subsequently accomplished by absorption of ArF radiation. This spectrum is a summation of 500 shots.

fer in reduced mass by 2.3%, resulting in a significant isotope shift. Moreover, these species occur at the same total mass, resulting in a doubling of the vibronic features in mass 254, as compared to mass 252 or 253. As is discussed more fully below, the consideration of isotope shifts is very helpful in the analysis of complicated vibronic spectra, and has enabled a definite numbering of the vibrational levels in the progressions observed in the spectra of NiPt.

B. Vibronic spectra

The resonant two-photon ionization spectrum of jet-cooled NiPt shows numerous vibronic bands over the spectral range 13 500–22 600 cm^{-1}. Examination of the spectrum shows that it can be broken up into two distinct regions based on the density of vibronic bands. In the red region of the spectrum (13 500–19 000 cm^{-1}) a number of weak, unassignable features are present, but the spectrum is dominated by intense bands which fit into three regular progressions. Figure 2 displays systems I and II, for each of which seven vibronic bands have been identified. Figure 3 displays the much more extensive progression of system III, for which 13 vibronic bands have been identified. In the blue region of the spectrum (19 000–22 600 cm^{-1}) the pattern of vibronic features becomes progressively more dense, with the vibronic band density reaching approximately 1 band/8 cm^{-1}. At 22 567 cm^{-1} the spectrum suddenly and dramatically ends. This is discussed more fully in Sec. III C below, where 22 567 cm^{-1} is identified as the dissociation limit of NiPt.

The assignment of vibrational quantum numbers in systems I, II, and III has been aided considerably by the measurement of isotope shifts in the various bands. As discussed in Sec. III A above, masses 252 and 253 are essentially pure species, consisting almost entirely of $^{58}Ni^{194}Pt$ and $^{58}Ni^{195}Pt$, respectively. Moreover, these species have nearly the same reduced mass, so the isotope shift is expected to be quite small, as is observed in our spectra. On the other hand, mass 254 contains contributions from both $^{58}Ni^{196}Pt$ and $^{60}Ni^{194}Pt$, which differ in reduced mass by 2.3%. Thus, as

TABLE I. Isotopic modifications of NiPt.

Mass	Intensity[a]	Combination	% Contribution[b]	Reduced mass[c]
250	0.53	$^{58}Ni^{192}Pt$	99.36	44.51
		$^{60}Ni^{190}Pt$	0.64	45.56
252	22.54	$^{58}Ni^{194}Pt$	99.09	44.61
		$^{60}Ni^{192}Pt$	0.91	45.67
253	22.95	$^{58}Ni^{195}Pt$	99.96	44.67
		$^{61}Ni^{192}Pt$	0.04	46.25
254	25.83	$^{58}Ni^{196}Pt$	66.48	44.72
		$^{60}Ni^{194}Pt$	33.41	45.78
		$^{62}Ni^{192}Pt$	0.11	46.82
255	9.26	$^{60}Ni^{195}Pt$	95.77	45.84
		$^{61}Ni^{194}Pt$	4.23	46.37
256	13.15	$^{58}Ni^{198}Pt$	37.23	44.82
		$^{60}Ni^{196}Pt$	50.48	45.89
		$^{61}Ni^{195}Pt$	3.06	46.42
		$^{62}Ni^{194}Pt$	9.16	46.94
		$^{64}Ni^{192}Pt$	0.06	47.96
257	1.54	$^{61}Ni^{196}Pt$	19.57	46.48
		$^{62}Ni^{195}Pt$	80.43	47.00
258	3.17	$^{60}Ni^{198}Pt$	59.61	46.00
		$^{62}Ni^{196}Pt$	29.19	47.06
		$^{64}Ni^{194}Pt$	11.20	48.08
259	0.45	$^{61}Ni^{198}Pt$	19.03	46.59
		$^{64}Ni^{195}Pt$	80.97	48.14
260	0.54	$^{62}Ni^{198}Pt$	49.13	47.17
		$^{64}Ni^{196}Pt$	50.87	48.20

[a] Defined as the percentage of NiPt molecules having the prescribed integer mass. Intensities below 0.1% are omitted.

[b] Defined as the percentage of NiPt molecules of a given mass having the prescribed combination of isotopes. Contributions below 0.04% are omitted.

[c] Masses given in amu, based on $^{12}C = 12.000\,000\,00$, as compiled in Ref. 32.

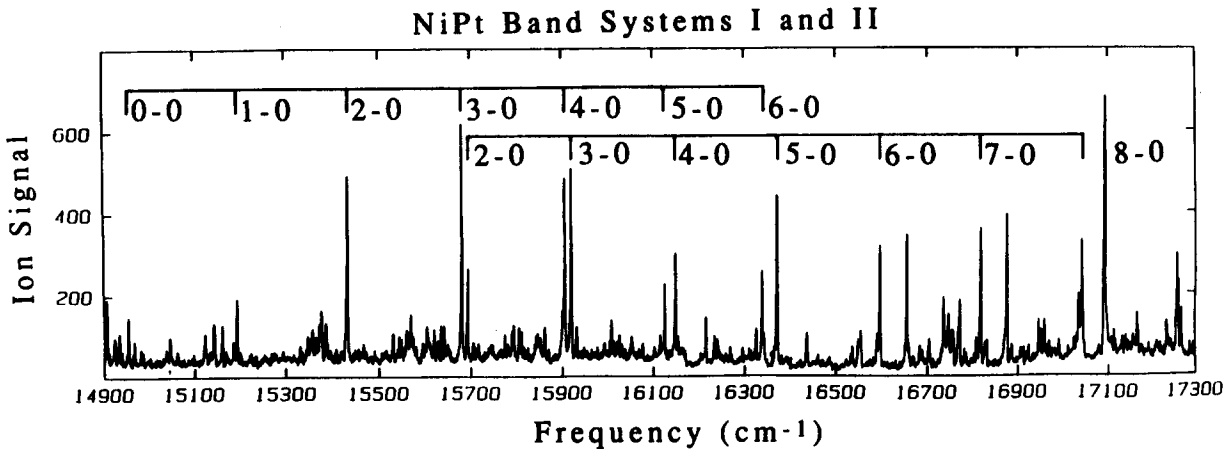

FIG. 2. Resonant two-photon ionization optical spectrum of $^{58}Ni^{195}Pt$ showing systems I and II. Absolute vibrational numbering of the bands was made possible by analysis of the isotope shifts (see Table II and Fig. 4). This figure is a composite of several scans employing the dyes rhodamine 610 and 640, DCM, rhodamine 640/DCM mix, and LDS 698 in conjunction with ArF radiation as the photoionization laser.

one increases the upper state vibrational quantum number v', the v'–0 bands in mass 254 split apart, with the higher frequency component arising from $^{58}Ni^{196}Pt$ and the lower frequency component arising from $^{60}Ni^{194}Pt$. Moreover, based on the percent contributions of $^{58}Ni^{196}Pt$ (66.48%) and $^{60}Ni^{194}Pt$ (33.41%) to mass 254, the ratio of intensities of the high frequency component to the low frequency component should be approximately 2:1. This splitting is illustrated in Fig. 4, where the 4–0 and 5–0 bands of system I and the 3–0 and 4–0 bands of system II are shown for both mass 253 ($^{58}Ni^{195}Pt$) and mass 254 ($^{58}Ni^{196}Pt$, and $^{60}Ni^{194}Pt$).

Using the measured band positions, vibrational analyses were performed by fitting the data to[33]

$$\nu = \nu_{00} + \omega_e' v' - \omega_e' x_e' (v'^2 + v'). \tag{3.1}$$

Isotope shifts were measured from the data for mass 254, (obtained in low resolution), and were compared to calculated isotope shifts obtained from the formula[33]

$$\Delta\nu^i = \nu - \nu^i = \omega_e' v' (1-\rho) - \omega_e' x_e' (v'^2 + v')(1-\rho^2). \tag{3.2}$$

In this formula, ν refers to the frequency of the v'–0 band of a species of reduced mass μ, and ν^i refers to the frequency of the corresponding band in the isotopic modification with reduced mass μ^i. The constants ω_e' and $\omega_e' x_e'$ refer to the reference species with reduced mass μ, and ρ is given by

$$\rho = (\mu/\mu^i)^{1/2}. \tag{3.3}$$

It should also be emphasized that formula (3.2) assumes that the isotope shift of the origin band ($v' = v'' = 0$) is zero. Since the isotope shift of an origin band lies below our experimental resolution (in low-resolution scans, at least), the use of (Eq. 3.2) is justified. Using Eq. (3.2), the absolute vibrational numbering of systems I, II, and III was varied to obtain the best agreement between the measured and calculated isotope shifts. The resulting assignments are given in

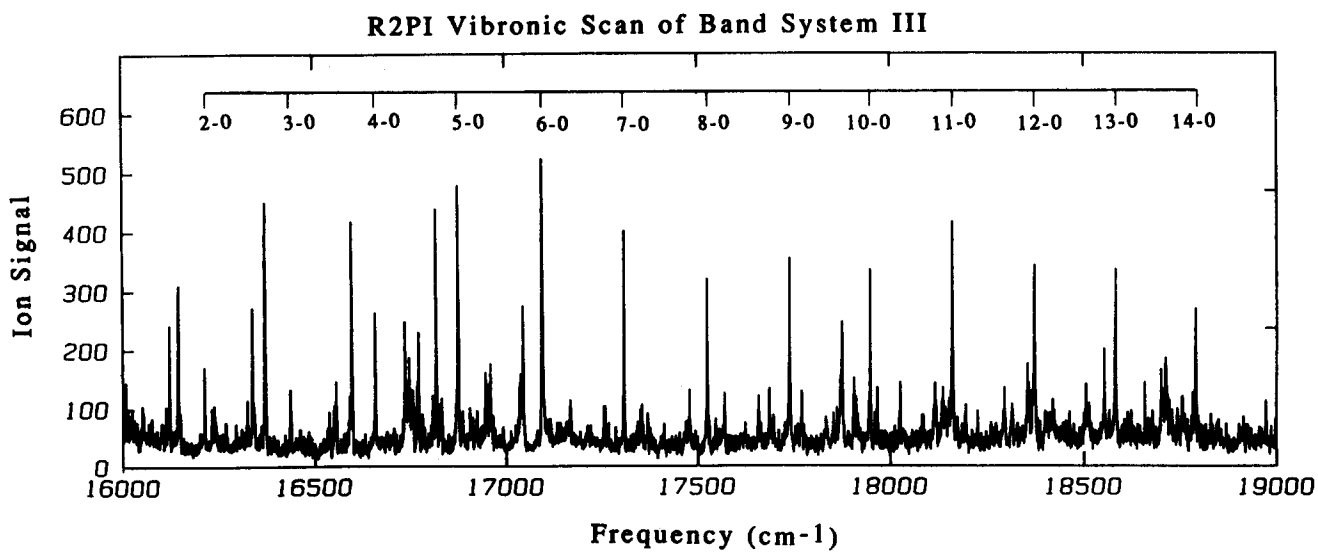

FIG. 3. Resonant two-photon ionization optical spectrum of $^{58}Ni^{195}Pt$ showing all bands of system III. This figure is a composite of five different scans using coumarin 540A, rhodamines 610 and 640, DCM, and a rhodamine 640/DCM mix. All scans used the ArF excimer laser as the ionization source. Absolute vibrational numbering of the bands was again made possible by analysis of the isotope shifts between $^{58}Ni^{196}Pt$ and $^{60}Ni^{194}Pt$, both of which occur in mass 254.

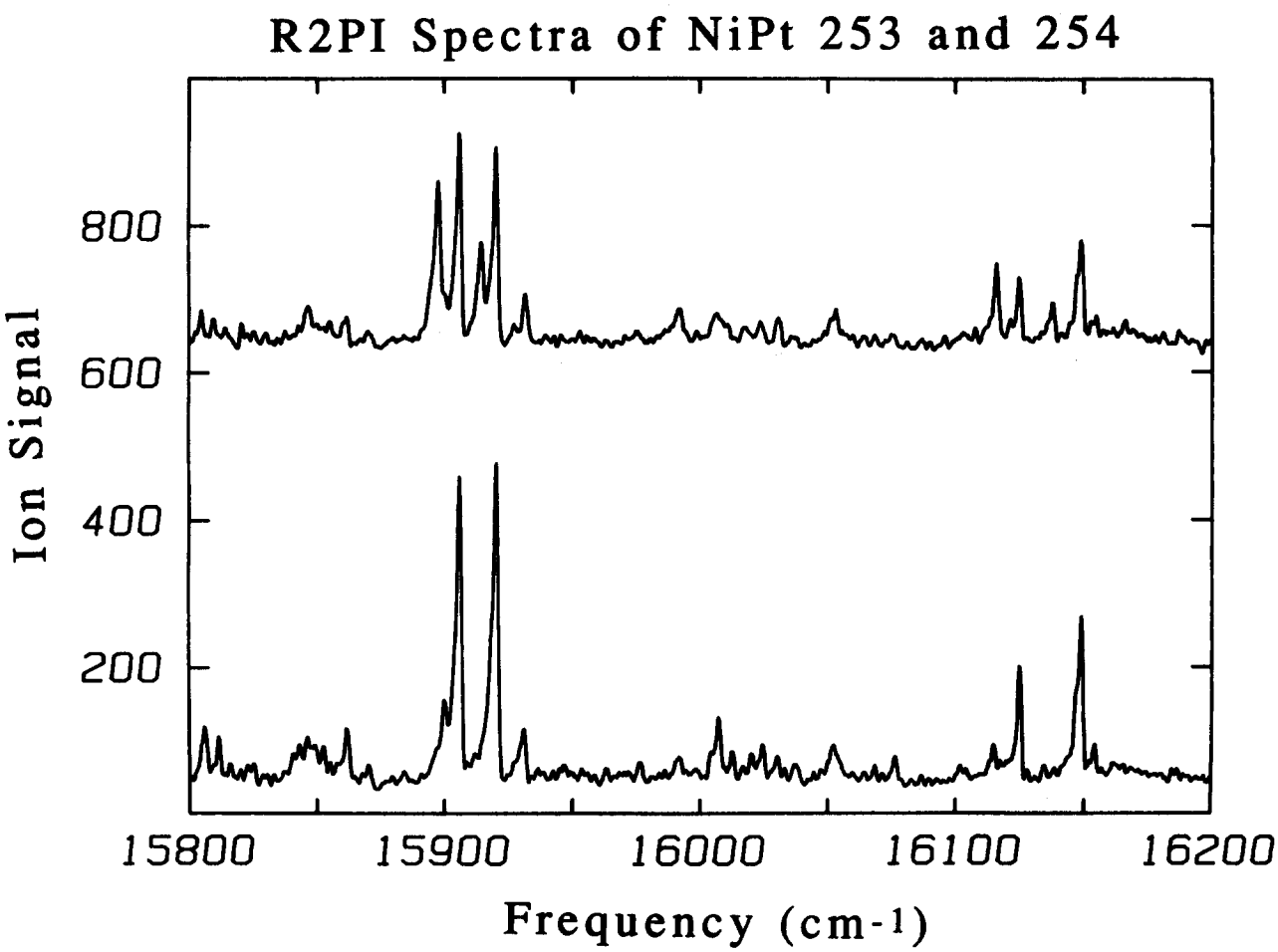

FIG. 4. Resonant two-photon ionization spectra of the mass 253 ($^{58}Ni^{195}Pt$) signal (lower panel) and of the mass 254 (66.48% $^{58}Ni^{196}Pt$, 33.41% $^{60}Ni^{194}Pt$) signal (upper panel). The latter species shows isotopic splittings due to the 2.3% difference in reduced mass between the two components. Measurements of these isotopic splittings enabled a definite vibrational numbering to be assigned in systems I, II, and III, as shown in Table II.

Table II, and spectroscopic constants for $^{58}Ni^{195}Pt$ are reported in Table III, assuming the vibrational numbering as given in Table II.

C. Dissociation energy of NiPt

As mentioned above, the density of vibronic features in the R2PI spectrum of NiPt becomes progressively greater as one moves toward the blue. This increasing spectral congestion continues with no sign of abatement until the spectrum abruptly terminates at 22 567 cm^{-1}, as shown in Fig. 5. Given the high density of states to the red of this limit, a comparable density of optically accessible states must exist to the blue of this value as well. It is simply inconceivable that a molecule possessing an optically accessible state every 10 cm^{-1} or so should suddenly show no spectral features whatsoever above a very sharp threshold energy, as observed in Fig. 5.

According to these arguments, the spectrum shown in Fig. 5 should not be possible. This spectrum may be explained however, if we note that we detect only a subset of the optically accessible upper states, namely those which live long enough to absorb an ArF photon, resulting in photoionization. Thus, rather than signaling the end of the optical spectrum, the threshold observed in Fig. 5 presumably signals the beginning of an energy range in which rapid decay of the excited state occurs. Based on a painstaking scan of the 22 600–23 600 cm^{-1} range, with the dye laser and ArF excimer laser carefully overlapped in time, it may be concluded that no optically accessible states in this region have lifetimes exceeding 10 ns. In contrast, measurements of 11 randomly selected bands between 20 134 and 22 567 cm^{-1} (including the last observed band at 22 567 cm^{-1}) show lifetimes of 2.1–4.2μs, as measured by time-delayed resonant two-photon ionization methods. At the precise energy of 22 567 cm^{-1} the lifetime of the excited states of the NiPt drops by a factor of approximately 1000, if not more.

It is unlikely that the strength of radiative coupling between the excited states and low-lying states suddenly increases by three orders of magnitude at precisely 22 567 cm^{-1}. On the other hand, it is quite possible that this threshold corresponds to the onset of a nonradiative decay mechanism in NiPt. In an isolated diatomic molecule the only such process is predissociation, since below the true dissociation limit there is an insufficient density of states for true irrevers-

TABLE II. Vibronic bands of $^{58}Ni^{196}Pt$.[a]

v'	ν(observed)[b]	ν(calculated)[b,c]	Error	$\Delta\nu^j$ (observed)[b]	$\Delta\nu^j$ (calculated)[b,d]
System I					
0	14 985.63	14 983.98	1.65	...	...
1	15 224.37	15 226.62	− 2.25	2.21	2.76
2	15 462.16	15 463.63	− 1.47	4.46	5.38
3	15 697.00	15 695.04	1.96	7.21	7.86
4	15 921.57	15 920.82	0.75	7.40	10.20
5	16 140.88	16 141.00	− 0.12	8.74	12.40
6	16 355.05	16 355.56	− 0.51	13.13	14.46
System II					
2	15 709.89	15 709.95	− 0.06	0.00	5.28
3	15 936.37	15 937.04	− 0.67	5.38	7.89
4	16 164.43	16 163.12	1.31	10.77	10.48
5	16 387.87	16 388.18	− 0.31	12.72	13.05
6	16 612.90	16 612.23	0.67	16.73	15.37
7	16 833.34	16 835.27	− 1.93	16.50	18.13
8	17 058.30	17 057.30	1.00	21.51	20.64
System III					
2	16 231.54	16 231.57	− 0.04	3.57	5.19
3	16 452.92	16 452.92	0.00	7.33	7.78
4	16 673.24	16 672.99	0.25	9.62	10.36
5	16 891.07	16 891.80	− 0.73	13.28	12.94
6	17 110.17	17 109.34	0.83	15.40	15.52
7	17 324.74	17 325.62	− 0.88	16.94	18.09
8	17 541.51	17 540.62	0.89	21.55	20.66
9	17 755.52	17 754.36	1.16	23.20	23.22
10	17 964.87	17 966.83	− 1.97	24.18	25.78
11[e]	18 177.58	18 178.04	− 0.46	...	...
12[e]	18 389.00	18 387.98	1.02	...	...
13[e]	18 596.77	18 596.65	0.12	...	...
14[e]	18 803.85	18 804.05	− 0.20	...	...

[a] All observed bands originate from $v'' = 0$.

[b] All numerical values are in wave numbers (cm^{-1}).

[c] The band positions were fitted via a least-squares treatment of $\nu = \nu_{00} + \omega_e' v' - \omega_e' x_e' (v' + v'^2)$, where ν_{00} is the band origin, ω_e' is the fundamental frequency, and $\omega_e' x_e'$ is the anharmonicity.

[d] The calculated isotope shift $\Delta\nu^j$, was found by assuming the shift of the band origins was zero and employing the formula $\Delta\nu^j = \omega_e' v' (1 - \rho) - \omega_e' x_e' (v' + v'^2)(1 - \rho^2)$, where $\rho = (\mu/\mu_i)^{1/2}$ and μ and μ_i are the reduced masses of the $^{58}Ni^{196}Pt$ and $^{60}Ni^{194}Pt$ isotopes, respectively.

[e] The peak intensity for these bands are reduced compared to the others and since the $^{60}Ni^{194}Pt$ isotope contributes only 33% to the mass peak intensity (see Table I) it was difficult to observe band positions in this region of the spectrum for this isotope.

TABLE III. Spectroscopic constants of $^{58}Ni^{195}Pt$.

	Band systems		
Property	I[c]	II[c]	III[c]
ν_{00}[a,b]	14 983.43 ± 2.13	15 248.39 ± 4.88	15 784.52 ± 1.36
ω_e'[a,b]	248.50 ± 1.92	232.81 ± 2.14	225.37 ± 0.41
$\omega_e' x_e'$[a,b]	2.82 ± 0.27	0.76 ± 0.18	0.64 ± 0.02
B_0''[a]	...	...	0.077 44 ± 0.000 16
r_0''[a]	...	...	2.207 8 ± 0.002 3
B_e'[a]	...	...	0.068 96 ± 0.000 23
α_e'[a]	...	...	0.000 68 ± 0.000 26
r_e'[a]	...	...	2.339 6 ± 0.003 9

[a] All constants reported in this table are given in wave numbers (cm^{-1}), except r_0 and r_e which are given in angstroms (Å). All error limits represent one standard deviation (1σ).

[b] The band origin ν_{00}, fundamental ω_e', and the anharmonicity $\omega_e' x_e'$ of the upper electronic states were obtained by fitting a linear least-squares treatment of $\nu = \nu_{00} + \omega_e' v' - \omega_e' x_e' (v' + v'^2)$.

[c] For band systems I and II, the absolute frequency of the band origins are expected to be accurate within ± 15 cm^{-1} due to the uncertainty in the calibration of the dye laser used in this work. The relative uncertainty between the band origins is much smaller, estimated as ± 2 cm^{-1}. The band origin for system III is probably accurate to the quoted uncertainty, since an iodine cell was simultaneously scanned for the 6–0 and 8–0 bands of this system.

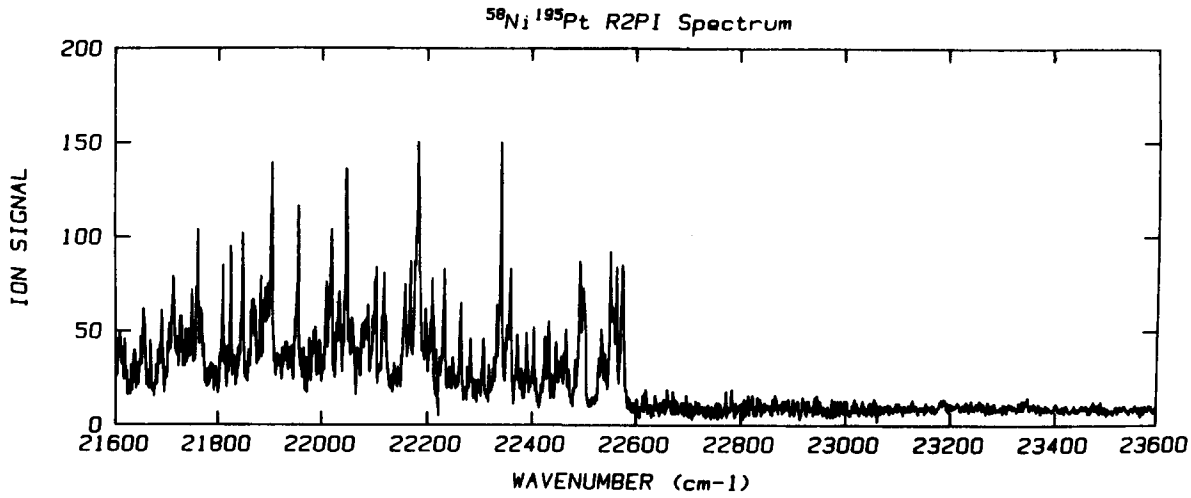

FIG. 5. Resonant two-photon ionization spectrum of the $^{58}Ni^{195}Pt$ isotopic combination at the lowest dissociation threshold ($D_0 = 2.798 \pm 0.003$ eV). This spectrum is a composite of two scans using coumarin 440 and stilbene 420, with ArF radiation as the photoionization laser. The sharp cutoff in the spectrum above 22 567 cm^{-1} is due to rapid predissociation which sets in above this threshold. The lifetime of the highest frequency band that is observed is $3.1 \pm 0.4\mu s$, while dissociation above 22 567 cm^{-1} must occur with a lifetime below 10 ns.

ible decay to occur. Thus, the sudden lack of observable transitions above 22 567 cm^{-1} results from a rapid predissociation ($\tau \leqslant 5$ ns) which proceeds more rapidly than photoionization. Moreover, given the sudden onset of this process and the vast number of accessible excited electronic states in this energy range (as judged by the density of vibronic bands at the red end of Fig. 5), we suggest that the observed threshold corresponds to the true dissociation energy of NiPt. This suggestion is based on the idea that the number of electronic states which are energetically accessible at the dissociation limit is so vast that motion on a single Born–Oppenheimer potential energy surface becomes a very poor approximation indeed. Thus, as soon as one exceeds the lowest dissociation threshold in a molecule such as NiPt, the molecular eigenstate that is excited is a superposition of bound and unbound states, and predissociation occurs.

The mechanism of predissociation in open d-shell diatomics such as NiPt arises from perturbations between the huge number of potential energy surfaces near the lowest dissociation limit. To give some indication of the number of potential curves which are present, consider the lowest separated atom limit of NiPt, Ni $^3F_4$ + Pt $^3D_3$. In Hund's case (c), in which potential curves are labeled by the good quantum number Ω (and for $\Omega = 0$, by $+/-$), this separated atom limit leads to 35 potential energy surfaces, including 3 $\Omega = 0^+$ states, 4 $\Omega = 0^-$ states, 7 $\Omega = 1$ states, 6 $\Omega = 2$ states, 5 $\Omega = 3$ states, 4 $\Omega = 4$ states, 3 $\Omega = 5$ states, 2 $\Omega = 6$ states, and one state with $\Omega = 7$. In addition to the 35 potential energy curves which arise from this lowest separated atom limit, many more arise from low-lying excited states of the separated atoms, and many of these will be bound sufficiently to be energetically accessible at the lowest dissociation threshold.

Although accurate quantum chemical calculations of relativistic adiabatic potential energy curves for a molecule such as NiPt are quite difficult in the region near r_e, it is straightforward to determine the states which arise at the separated atom limit. In general, combination of two unlike atoms (with an even number of electrons altogether) with total angular momenta $(\mathbf{L}+\mathbf{S})$ of J_1 and J_2 leads to $(2J_< + 1)(J_> + 1)$ distinct Hund's case (c) potential curves, where $J_<$ and $J_>$ are the lesser and greater of J_1 and J_2, respectively. Thus by listing the known energy levels of the separated atoms[34] and computing the number of case (c) potential curves arising from each separated atom limit, one may obtain an idea of the expected density of electronic states in the diatomic molecule. Figure 6 presents the running sum of states $N(E)$ as a function of energy above the lowest dissociation limit for NiPt, along with Ni_2 and Pt_2 for comparison. In the figure $N(E)$ is the total number of Hund's case (c) potential curves lying in the range from zero energy (ground state separated atoms) up to E, evaluated at the separated atom limit. For NiPt each separated atom limit contributes $(2J_< + 1)(J_> + 1)$ potential curves to this sum; for Ni_2 and Pt_2 each separated atom limit contributes $(2J + 1)(J + 1)$ potential curves if the limit corresponds to atoms in *like* states, or $2(2J_< + 1(J_> + 1)$ potential curves if the limit corresponds to atoms in unlike states.

As is evident in Fig. 6, all three species (Ni_2, NiPt, and Pt_2) possess hundreds of potential curves within 2000 cm^{-1} of the lowest separated atom limit. When one considers that many of these potential curves have potential energy minima lying below the lowest dissociation limit, it is not surprising that the spectrum of NiPt just below the dissociation limit is quite congested (Fig. 5); nor is it surprising that as soon as one exceeds the dissociation threshold, predissociation sets in with rates greater than 10^8 s^{-1}. With these thoughts in mind, the observed threshold at 22 567 cm^{-1} may be used to evaluate the dissociation energy of NiPt, given by $D_0(\text{NiPt}) = 2.798 \pm 0.003$ eV.

D. Ionization potential of NiPt

Investigations of the resonant two-photon ionization spectrum of NiPt using ArF radiation show relatively strong transitions as far to the red as 14 100 cm^{-1} (1.748 eV). This

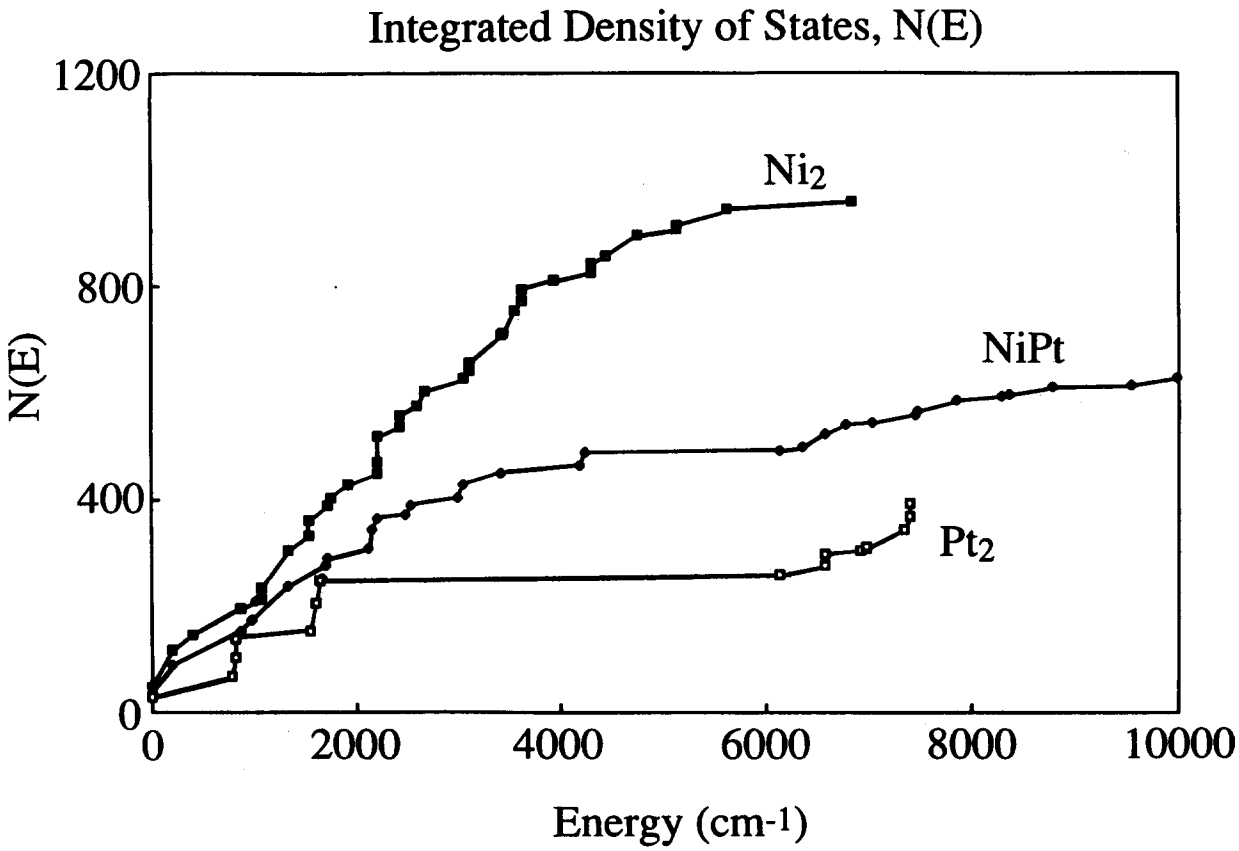

FIG. 6. Integrated density of states $N(E)$ vs E for Ni_2, NiPt, and Pt_2. In this figure $N(E)$ represents the number of distinct Hund's case (c) potential curves which arise from the interaction of two atoms with total energy between zero (ground state atoms) and E, computed using the Wigner–Witmer rules (Ref. 33) and the atomic energy levels as compiled by Charlotte Moore (Ref. 34). Many of these potential curves will be bound relative to the lowest dissociation limit, leading to a high density of vibronically coupled states near the dissociation limit. Couplings between these states are responsible for the prompt dissociation which sets in as soon as D_0 is exceeded in all three dimers: Ni_2, NiPt, and Pt_2.

places the ionization potential of NiPt below 8.17 eV. Studies employing F_2 radiation (7.87 eV) also give resonant two-photon ionization spectra, thereby proving that IP(NiPt) > 7.87 eV. Based on these results, the ionization limit of NiPt may be placed in the range IP(NiPt) = 8.02 ± 0.15 eV. With the ionization potential and bond strength of NiPt in hand, simple thermodynamic cycles permit the evaluation of $D_0(Ni^+-Pt) = 2.41 \pm 0.15$ eV and $D_0(Ni-Pt^+) = 3.58 \pm 0.35$ eV, using the values of IP(Ni) = 7.633 eV[34] and IP(Pt) = 8.8 ± 0.2 eV.[24]

E. Rotationally resolved spectra of $^{58}Ni^{195}Pt$

With the aid of an intracavity etalon the linewidth of the dye laser was narrowed to 0.03 cm^{-1}, and high resolution scans of the 6–0 and 8–0 bands of system III were undertaken. In this region of the spectrum the I_2 absorption spectrum[30,31] is quite dense and serves as an excellent calibration of our 0.2187 cm^{-1} free spectral range etalon, which is in turn used to assign absolute frequencies to all of the observed features in the spectrum. Although the linewidth of the laser was approximately 0.03 cm^{-1}, the rms deviation of the fitted I_2 absorption lines from their known frequencies ranged from 0.004 to 0.009 cm^{-1} in our various scans, with a maximum deviation of 0.016 cm^{-1}. Based on these values, the expected error in measured line frequencies for strong, unblended lines of NiPt should be below ± 0.01 cm^{-1}.

The rotationally resolved scans of the 6–0 and 8–0 bands of system III are shown in Fig. 7 for the $^{58}Ni^{195}Pt$ isotopic modification, along with simulated spectra. The bands are degraded strongly to the red, and show only P and R branches. The absence of a Q-branch implies that both transitions correspond to an $\Omega' = 0 \leftarrow \Omega'' = 0$ transition in Hund's case (c), which is certainly the appropriate case for the intermetallic open d-shell transition metal dimers. The measured line positions were least-squares fitted to the formula

$$\nu = \nu_0 + B'J'(J'+1) - B''J''(J''+1), \qquad (3.4)$$

thereby providing values of ν_0 for both the 6–0 and 8–0 bands, B_0'',B_6', and B_8'. Measured and fitted line positions and residuals are given in Table IV. In both bands an excellent fit is obtained, with no residuals larger than ± 0.012 cm^{-1}. The resulting values of B_6' and B_8' may be combined to give $B_e' = 0.068\,96 \pm 0.000\,23$ cm^{-1} and $\alpha_e' = 0.000\,68 \pm 0.000\,26$ cm^{-1} for the $^{58}Ni^{195}Pt$ isotope of NiPt. These values then give $r_e' = 2.3396 \pm 0.0039$ Å. Using the measured values of B_0'' in both the 6–0 and 8–0 bands, the average value $B_0'' = 0.077\,436 \pm 0.000\,158$ cm^{-1} may be derived, thereby giving $r_0'' = 2.2078 \pm 0.0023$ Å. Since only $v'' = 0$ bands have been observed, α_e'' cannot be estimated for the ground state, and r_0'' cannot be corrected to give r_e''. Neither may the Pekeris relationship giving α_e'' in terms of B_e'', ω_e'', and $\omega_e''x_e''$ be employed, since neither ω_e'' nor $\omega_e''x_e''$ are known. Based on previous work on NiCu,[26] however, α_e''

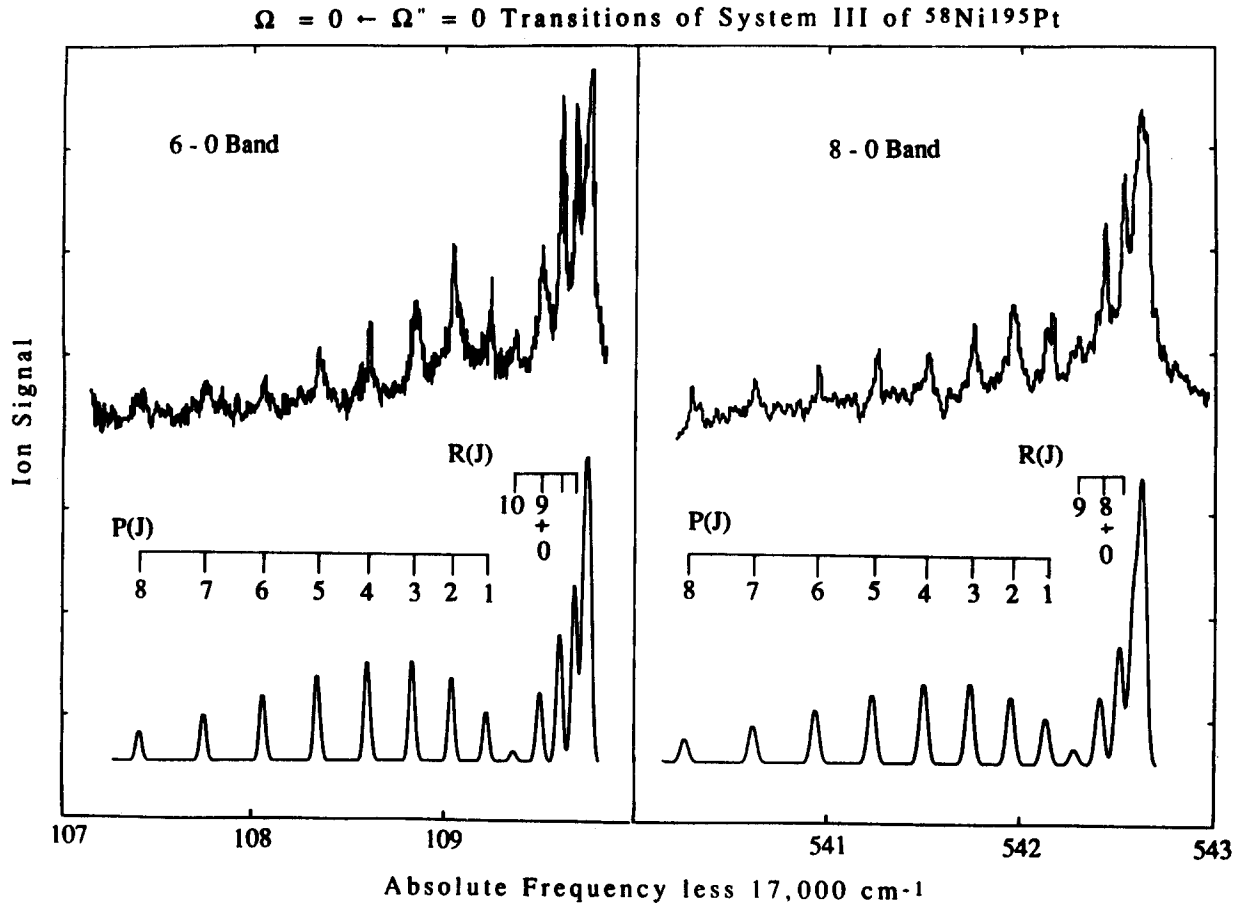

FIG. 7. High resolution (0.03 cm^{-1}) resonant two-photon ionization spectra of the 6–0 and 8–0 bands of system III for the $^{58}Ni^{195}Pt$ isotopic species. A bandhead is formed at low J in the R branch. The absence of a Q-branch forces the assignment as $\Omega' = 0 \leftarrow \Omega'' = 0$. The absolute frequency scale was established by simultaneously monitoring the transmission through an I_2 absorption cell, giving transitions which were assigned absolute wave numbers with the aid of the iodine atlas (Refs. 30 and 31). Shown below are simulated spectra, calculated with a laser linewidth of 0.03 cm^{-1} and a rotational temperature of 3 K.

for NiPt is probably less than 0.005 cm^{-1}, and r_e'' may be estimated as $r_e'' = 2.205 \pm 0.007$ Å. These values of r_e'' (2.205 Å) and r_e' (2.3396 Å) are consistent with the observed degradation of the bands to the red and with the lengthy progression of v'–0 bands which is shown in Fig. 3.

IV. DISCUSSION

With the fundamental spectroscopic constants and bond strength of NiPt now in hand, it is possible to consider the electronic structure of this molecule in some detail. Comparisons with previous data on Ni_2[22] and Pt_2[24], and with other transition metal dimers may be made as well, providing a sound frame of reference for understanding the metal–metal chemical bond in the late transition metals.

The ground atomic level of platinum is $5d^9 6s^1, {}^3D_3$, while the $3d^9 4s^1, {}^3D_3$ level of nickel lies only 204.786 cm^{-1} above the $3d^8 4s^2, {}^3F_4$ ground level.[34] Consequently, there is essentially zero promotion energy involved in combining these two atoms to form a sigma-bonded dimer in which the $6s$ orbital of Pt forms a chemical bond with the $4s$ orbital of Ni. Of course, there is probably some hybridization of these orbitals with the platinum $6p_z$ and $5d_{z^2}$ and the nickel $4p_z$ and (possibly) $3d_{z^2}$ orbitals, but the fundamental picture of a sigma-bonded dimer remains unchanged. The question first brought up in the Introduction still remains unanswered however: What is the role of the d-orbitals in the chemical bonding between the nickel and platinum atoms?

In an open d-shell diatomic such as NiPt, this question may be addressed most directly by comparing the molecule to its coinage metal analog CuAu. The coinage metals possess very stable ground atomic terms of $nd^{10}(n+1)s^1$, $^2S_{1/2}$, so the filled d shells prohibit any direct d-electron contributions to the chemical bond. Significant departures in bond length or bond strength of the nickel group dimers from their coinage metal analogs therefore imply some degree of d-electron participation in the chemical bonding. Comparisons of Ni_2, NiPt, and Pt_2 to the coinage analogs Cu_2, CuAu, and Au_2 are given in Table V. Chemical bonding in the remaining nickel group dimers NiPd, Pd_2, and PdPt differs somewhat from that found in Ni_2, NiPt, and Pt_2, owing to the $4d^{10}5s^0, {}^1S_0$ ground atomic level of Pd. Results for the palladium-containing dimers are presented and discussed in the following article.[36]

As is evident from Table V, Ni_2 and Cu_2 are nearly identical in bond strength and bond length, indicating little direct participation of the $3d$ electrons of nickel in the chemical bonding of Ni_2. Further evidence of the lack of d-electron bonding in Ni_2 is provided by the large value of $\Omega'' = 4$ for the ground electronic state of this species. Such a large

TABLE IV. Observed and fitted line positions for system III of $^{58}Ni^{195}Pt$.[a]

Assignment	Observed line position[b]	Fitted line position[c]	Residual	Comment
6–0 band[d]				
$P(1)$	9.239	9.229	0.010	
$P(2)$	9.043	9.048	−0.005	
$P(3)$	8.850	8.841	0.009	
$P(4)$	8.607	8.607	0.000	
$P(4)$	8.352	8.348	0.004	
$P(6)$	8.058	8.063	−0.005	
$P(7)$	7.760	7.751	0.009	
$P(8)$	7.404	7.414	−0.010	
$R(0)$	9.513	9.513	0.000	
$R(1)$	9.606	9.616	−0.010	
$R(2)$	9.687	9.693	−0.006	
$R(3)$	...	...	...	R bandhead
$R(4)$	...	...	...	R bandhead
$R(5)$	...	...	...	R bandhead
$R(6)$	...	...	...	blended with $R(2)$
$R(7)$	9.687	9.687	0.000	
$R(8)$	...	...	...	blended with $R(1)$
$R(9)$	9.513	9.502	0.011	
$R(10)$	9.365	9.371	−0.006	
8–0 band[d]				
$P(1)$	42.158	42.148	0.010	
$P(2)$	41.956	41.965	−0.009	
$P(3)$	41.754	41.754	0.000	
$P(4)$	41.517	41.515	0.002	
$P(5)$	41.250	41.247	0.003	
$P(6)$	40.947	40.951	−0.004	
$P(7)$	40.614	40.626	−0.012	
$P(8)$	40.285	40.273	0.012	
$R(0)$	42.426	42.429	−0.003	
$R(1)$	42.526	42.527	−0.001	
$R(2)$	...	...	...	R bandhead
$R(3)$	...	...	...	R bandhead
$R(4)$	...	...	...	R bandhead
$R(5)$	...	...	...	R bandhead
$R(6)$	...	...	...	R bandhead
$R(7)$	42.526	42.521	0.005	
$R(8)$	42.426	42.421	0.005	
$R(9)$	42.293	42.292	0.001	
$R(10)$	41.128	42.136	−0.008	

[a] All numerical values are in wave numbers (cm^{-1}).

[b] The observed line positions are absolute and were measured by calibrating with the absorption spectrum of I_2, which was scanned simultaneously.

[c] Fitted line positions are obtained by a least-squares fit of the observed line positions for each individual band to the formula $\nu = \nu_0 + B' J'(J'+1) - B'' J''(J''+1)$. From the fit of the 6–0 band, we obtain $\nu_0 = 17\,109.3841 \pm 0.032$ cm_$^{-1}$, $B_0'' = 0.077\,551 \pm 0.000\,228$ cm^{-1}, $B_6' = 0.064\,527 \pm 0.000\,194$ cm^{-1} and $\nu_0 = 17\,542.3031 \pm 0.0033$ cm^{-1}, $B_0'' = 0.077\,320 \pm 0.000\,218$ cm^{-1}, $B_8' = 0.063\,164 \pm 0.000\,179$ cm^{-1} from a fit of the 8–0 band. The small uncertainties, small residuals, and agreement between two independent fits of B_0'' support the assignment given.

[d] Absolute line positions are obtained by adding 17 100 cm^{-1} to the 6–0 band and 17 500 cm^{-1} to the 8–0 band.

value of Ω implies that the two $3d$ holes in Ni_2 occur in d orbitals of high angular momentum, since only $\delta\delta$ or $\pi\delta$ combinations of $3d$ holes can result in $\Omega'' = 4$. If $3d$ contributions to the chemical bonding in Ni_2 were very significant, one would expect the $3d$ orbitals to split into σ, π, δ, δ^*, π^*, and σ^* bonding and antibonding molecular orbitals, and the ground state would place the two $3d$ holes in the σ^* antibonding orbital, which should lie highest in energy. This would give a $^1\Sigma_g^+$ ground state for Ni_2, which would possess $\Omega'' = O_g^+$. Instead of bonding considerations, it appears that d-electron correlation and $3d$–$4s$ hybridization effects are dominant in determining the ground state of Ni_2.[37–40]

Diatomic platinum, on the other hand, shows a bond strength 0.85 eV greater than its coinage metal analog Au_2.[24] This is a very significant effect, and unequivocally demonstrates the importance of $5d$ contributions to the bonding in Pt_2. In this case neither the bond length nor the value of Ω'' are yet known, but one would expect a substantially shorter bond in Pt_2 than in Au_2, and Pt_2 would be expected to have a ground state characterized by $\Omega'' = O_g^+$ as well. *Ab initio* calculations[41,42] on Pt_2 have predicted either an $\Omega'' = 4_g$ or an $\Omega'' = O_g^+$ ground state, in both cases placing the d holes in δ orbitals ($\delta\delta$ configuration of holes). This appears to be at odds with the experimentally deter-

TABLE V. Comparisons of the nickel group and coinage group dimers.

Nickel group dimer	Coinage group dimer	Δ^i
Ni_2	Cu	
$r_0 = 2.200 \pm 0.007$ Å[2]	$r_e = 2.2197$ Å[b]	0.058
$D_0 = 2.068 \pm 0.01$ eV[a]	$D_0 = 2.01 \pm 0.08$ eV[c]	± 0.08 eV
$\Omega'' = 4$[a]	$^1\Sigma_g^+$	
NiPt	CuAu	
$r_0 = 2.2078 \pm 0.0023$ Å[d]	$r_e = 2.330 \pm 0.003$ Å[e]	0.458
$D_0 = 2.798 \pm 0.003$ eV[d]	$D_0 = 2.34 \pm 0.10$ eV[c]	± 0.10 eV
$\Omega'' = 0$[d]	$^1\Sigma^+$	
Pt_2	Au_2	
$r_0 = ?$	$r_e = 2.4719$ Å[g]	0.85
$D_0 = 3.14 \pm 0.02$ eV[f]	$D_0 = 2.29 \pm 0.02$ eV[h]	± 0.03 eV
$\Omega'' = ?$	$^1\Sigma_g^+ (O_g^+)$	

[a] Reference 22.
[b] Reference 23.
[c] Reference 3.
[d] This work.
[e] Reference 43.
[f] Reference 24.
[g] Reference 35.
[h] Reference 25.
[i] Δ is defined as the bond strength of the nickel group dimer minus the bond strength of its filled d-shell analog. It provides an estimate of the contribution to the bond strength in the nickel group dimer due to d-electron bonding.

mined bond strength of Pt_2.[24] The $5d$ orbitals may well be found to play a more important role in the chemical bonding of Pt_2 at a higher level of theory.

The mixed dimer, NiPt, shows a bond strength 0.46 eV greater than its coinage metal analog CuAu. In what may be a fortuitous coincidence, this is almost exactly equal to the average of the d-electron contributions to the bond strength of Ni_2 (0.058 eV) and Pt_2 (0.85 eV). A second indication of significant d-orbital contributions to the bonding in NiPt may be found in the measured bond length ($r_0'' = 2.208 \pm 0.002$ Å), which within the error limits is identical to that of Ni_2 (2.200 ± 0.007 Å). A recent determination of the bond length of CuAu has provided $r_0(\text{CuAu}) = 2.330 \pm 0.003$ Å.[43] Thus the d-orbital contributions to the bonding in NiPt reduce the bond length by approximately 0.12 Å as compared to what might be expected in the absence of such effects. Finally, although it is by no means definitive, the low value of $\Omega'' = 0$ for the NiPt ground state is consistent with significant d-orbital participation in the chemical bond.

The general appearance of the low-resolution spectra of NiPt, in the red region of the spectrum (13 500–19 000 cm^{-1}), is also consistent with d-orbital participation in the chemical bond. The observed spectra of NiPt are relatively sparse as compared to Ni_2,[22] which displays a near-continuum in this spectral range. This (relative) sparsity of band systems is consistent with a picture in which the d orbitals are split into σ, π, δ, δ^*, π^*, and σ^* bonding and antibonding pairs, thereby spreading the large number of electronic states associated with the open d shells over a broader range of energy than occurs in Ni_2. In this respect the low-resolution spectrum of NiPt in the range 13 500–19 000 cm^{-1} is quite reminiscent of that found for Pt_2.[24]

V. CONCLUSION

A resonant two-photon ionization spectroscopic study of NiPt has revealed strong evidence of d-electron participation in the bonding of this molecule. A rich vibronic spectrum has been found over the range 13 500–22 567 cm^{-1}. The spectrum consists of a relatively sparse region from 13 500–19 000 cm^{-1}, in which three vibronic progressions have been located and analyzed. Further to the blue the spectrum becomes progressively more dense, ultimately terminating at 22 567 cm^{-1} where the R2PI spectrum abruptly comes to an end. Time-delayed two-photon ionization techniques have been employed, demonstrating that at this threshold the lifetimes of the excited states drop from approximately 3 μs to below 10 ns, indicating the onset of rapid predissociation above this energy. Based on the abrupt onset of predissociation, the total lack of observed transitions to the blue of this threshold, and the large density of states to the red of this threshold, it is proposed that 22 567 cm^{-1} corresponds to the true dissociation limit, thereby providing $D_0(\text{NiPt}) = 2.798 \pm 0.003$ eV. Resonant two-photon ionization studies employing the ArF (6.42 eV) and F_2 (7.87 eV) excimer transitions place the ionization potential of NiPt at IP(NiPt) $= 8.02 \pm 0.15$ eV. In combination with $D_0(\text{NiPt})$ and the atomic ionization potentials this then implies $D_0(\text{Ni}^+\text{–Pt}) = 2.41 \pm 0.15$ eV, $D_0(\text{Ni–Pt}^+) = 3.58 \pm 0.35$ eV.

High resolution (0.03 cm^{-1}) studies of the 6–0 and 8–0 bands of system III demonstrate that this system is an

$\Omega' = 0 \leftarrow \Omega'' = 0$ system, and give bond lengths of the upper and lower states of $r'_e = 2.3396 \pm 0.0039$ Å and $r''_0 = 2.208 \pm 0.002$ Å, respectively. The bond length of the ground state is identical to that of Ni_2, within experimental error, and is 0.12 Å shorter than found for CuAu. This short bond length implies significant d-orbital interactions in NiPt. In addition, D_0(NiPt) is 0.46 eV greater than D_0 (CuAu), again implying a definite bonding contribution from the d electrons in this molecule.

ACKNOWLEDGMENTS

We are grateful to Professor William H. Breckenridge for the use of the intracavity etalon and accessories employed in the high resolution studies. We also gratefully acknowledge research support from the National Science Foundation, under Grant No. CHE-85-21050. Acknowledgement is also made to the donors of the Petroleum Research Fund, administered by the ACS, for partial support of this research.

[1] F. A. Cotton and R. A. Walton, *Multiple Bonds Between Metal Atoms* (Wiley, New York, 1982).
[2] W. Weltner, Jr. and R. J. Van Zee, Annu. Rev. Phys. Chem. **35**, 291 (1984).
[3] M. D. Morse, Chem. Rev. **86**, 1049 (1986).
[4] J. Koutecký and P. Fantucci, Chem. Rev. **86**, 539 (1986).
[5] D. R. Salahub, Adv. Chem. Phys. **69**, 447 (1987).
[6] I. Shim, Mat.-Fys. Meddr. Danske Vidensk. Selsk. (16 Res. Rep. of Niels Bohr Fellows) **41**, 147 (1985).
[7] S. R. Langhoff and C. W. Bauschlicher, Jr., Annu. Rev. Phys. Chem. **39**, 181 (1988).
[8] P. R. R. Langridge-Smith, M. D. Morse, G. P. Hansen, and R. E. Smalley, J. Chem. Phys. **80**, 593 (1984).
[9] Y. M. Efremov, A. N. Samoilova, and L. V. Gurvich, Opt. Spectrosc. **36**, 381 (1974).
[10] D. L. Michalopoulos, M. E. Geusic, S. G. Hansen, D. E. Powers, and R. E. Smalley, J. Phys. Chem. **86**, 3914 (1982).
[11] V. E. Bondybey and J. H. English, Chem. Phys. Lett. **94**, 443 (1983).
[12] S. J. Riley, E. K. Parks, L. G. Pobo, and S. Wexler, J. Chem. Phys. **79**, 2577 (1983).
[13] Y. M. Efremov, A. N. Samoilova, V. B. Kozhukhovsky, and L. V. Gurvich, J. Mol. Spectrosc. **73**, 430 (1978).
[14] A. N. Samoilova, Y. M. Efremov, D. A. Zhuravlev, and L. V. Gurvich, Khim. Vys. Energ. **8**, 229 (1974).
[15] J. B. Hopkins, P. R. R. Langridge-Smith, M. D. Morse, and R. E. Smalley, J. Chem. Phys. **78**, 1627 (1983).
[16] C. Cossé, M. Fouassier, T. Mejean, M. Tranquille, D. P. DiLella, and M. Moskovits, J. Chem. Phys. **73**, 6076 (1980).
[17] S. K. Loh, L. Lian, and P. B. Armentrout, J. Am. Chem. Soc. **111**, 3167 (1989).
[18] S. K. Gupta, and K. A. Gingerich, J. Chem. Phys. **70**, 5350 (1979).
[19] L. Pauling, J. Chem. Phys. **78**, 3346 (1983).
[20] C. W. Bauschlicher, Jr., S. P. Walch, and P. E. M. Siegbahn, J. Chem. Phys. **78**, 3347 (1983).
[21] S. P. Walch and C. W. Bauschlicher, Jr. in *Comparison of Ab Initio Quantum Chemistry with Experiment*, edited by R. J. Bartlett (Reidel, Dordrecht, 1985) p. 17.
[22] M. D. Morse, G. P. Hansen, P. R. R. Langridge-Smith, L. -S. Zheng, M. E. Geusic, D. L. Michalopoulos, and R. E. Smalley, J. Chem. Phys. **80**, 5400 (1984).
[23] N. Åslund, R. F. Barrow, W. G. Richards, and D. N. Travis, Ark. Fys. **30**, 171 (1965).
[24] S. Taylor, G. W. Lemire, Y. Hamrick, Z. -W. Fu, and M. D. Morse, J. Chem. Phys. **89**, 5517 (1988).
[25] J. Kordis, K. A. Gingerich, and R. J. Seyse, J. Chem. Phys. **61**, 5114 (1974).
[26] Z. -W. Fu and M. D. Morse, J. Chem. Phys. **90**, 3417 (1989).
[27] G. W. Lemire, Z. -W. Fu, Y. Hamrick, S. Taylor, and M. D. Morse, J. Phys. Chem. **93**, 2313 (1989).
[28] Z. -W. Fu, G. W. Lemire, Y. Hamrick, S. Taylor, J. -C. Shui, and M. D. Morse, J. Chem. Phys. **88**, 3524 (1988).
[29] S. C. O'Brien, Y. Liu, Q. Zhang, J. R. Heath, F. K. Tittel, R. F. Curl, and R. E. Smalley, J. Chem. Phys. **84**, 4074, (1986).
[30] S. Gerstenkorn and P. Luc, *Atlas du Spectre d'Absorption de la Molécule d'Iode* (CNRS, Paris, 1978).
[31] S. Gerstenkorn and P. Luc, Rev. Phys. Appl. **14**, 791 (1979).
[32] J. H. E. Mattauch, W. Thiele, and A. H. Wapstra, Nucl. Phys. **67**, 1, 32, 73 (1965).
[33] G. Herzberg, *Molecular Spectra and Molecular Structure I. Spectra of Diatomic Molecules*, 2nd ed. (Van Nostrand Reinhold, New York, 1950).
[34] C. E. Moore, Natl. Bur. Stand. Circ. No. 467 (1971), Vols II and III.
[35] L. L. Ames and R. F. Barrow, Trans. Faraday Soc. **63**, 39 (1967).
[36] S. Taylor, E. M. Spain, and M. D. Morse, J. Chem. Phys. **92**, 2710 (1990).
[37] S. P. Walch and W. A. Goddard III, J. Am. Chem. Soc. **98**, 7908 (1976).
[38] T. H. Upton and W. A. Goddard III, J. Am. Chem. Soc. **100**, 5659 (1978).
[39] I. Shim, J. P. Dahl, and H. Johansen, Int. J. Quantum Chem. **15**, 311 (1979).
[40] J. O. Noell, M. D. Newton, P. J. Hay, R. L. Martin, and F. W. Bobrowicz, J. Chem. Phys. **73**, 2360 (1980).
[41] H. Basch, D. Cohen, and S. Topiol, Isr. J. Chem. **19**, 233 (1980).
[42] K. Balasubramanian, J. Chem. Phys. **87**, 6573 (1987).
[43] G. A. Bishea, J. C. Pinegar, and M. D. Morse (in preparation).